

Microstructure and thermal stability of ZrB₂ powder infiltrated by molten Cu and CuCr1Zr alloy

N. Beronská^{1*}, A. Opálek¹, Š. Nagy¹, T. Dvorák¹, T. Švantner¹, P. Švec², P. Štefánik¹,
K. Iždinský¹

¹*Institute of Materials and Machine Mechanics, Slovak Academy of Sciences,
Dúbravská cesta 9, 845 13 Bratislava, Slovak Republic*

²*Institute of Physics, Slovak Academy of Sciences, Dúbravská cesta 9, 845 11 Bratislava, Slovak Republic*

Received 20 December 2018, received in revised form 14 January 2019, accepted 14 January 2019

Abstract

Cu/ZrB₂ and CuCr1Zr/ZrB₂ composites were prepared by gas pressure infiltration technology. The ZrB₂ powder was used as reinforcement. No interfacial reaction took place for Cu, or CuCr1Zr matrix as confirmed by transmission electron microscopy (TEM). The thermal stability of composites was very good, i.e. without any indication of possible disintegration. Composites exhibit high structural stability when subjected to 5 consecutive heating/cooling cycles to 800 °C. Maximums of relative elongations recorded for particular heating/cooling cycles slightly increased for Cu/ZrB₂ composite and slightly decreased for CuCr1Zr/ZrB₂ composite. However, the differences are negligible.

Key words: Cu-ZrB₂ composite materials, metal matrix, ceramic powder, gas pressure infiltration, thermal expansion

1. Introduction

In a previous paper [1], Cu/ZrB₂ and CuCr1Zr/ZrB₂ composites were prepared using gas pressure infiltration method. ZrB₂ preforms were successfully infiltrated by molten metal. No substantial differences in the behaviour of composites had been observed given the non-reactive nature of bonding between copper metal and ZrB₂ ceramics. The composites exhibited high structural stability up to 800 °C.

Zirconium diboride (ZrB₂) is known as an ultra-high temperature ceramics. It has a very attractive combination of properties as high melting point (over 3200 °C), high thermal and electrical conductivity, high hardness, good strength, and chemical stability at high temperatures (high metallurgical stability, excellent corrosion resistance). The thermal conductivity of ZrB₂ increased from 56 W m⁻¹ K⁻¹ at room temperature to 67 W m⁻¹ K⁻¹ at 1675 K (1400 °C). It appeared to be very suitable material for applications that work under thermal stress, e.g. thermal protection components in hypersonic aerospace re-entry vehicles (wing's leading edges and nose caps), propul-

sion systems components, thermocouple sheaths, refractory crucibles, furnace heating elements, high-temperature electrodes for plasma applications and metal evaporator boats [1–5]. For thermal plasma processes, the most undesired feature is the high wear rate of used elemental electrodes. The development of a thermally stable type of spark-resistive material is still highly demanded. ZrB₂ ceramics in connection with copper seems to be an excellent spark-resistive material, resp. type of EDM electrode material [6–9].

Copper (Cu) with its high thermal conductivity (401 W m⁻¹ K⁻¹), good electrical conductivity, and availability is one of the best-known metals used for applications in electronics and electrical engineering [1]. Cu/ZrB₂ composite as an electrode in plasma applications was described in detail by Norasetthekul et al. [6]. To enhance the thermal conductivity of ZrB₂ ceramics the addition of Cu was necessary. As plasma struck the electrode surface, Cu melted and/or vaporized before ZrB₂. It was possible because of high thermal conductivity and low melting point (1083 °C) of Cu. Thus, excess heat was carried away from the surface by the Cu until the thermal stress on the ce-

*Corresponding author: tel.: +421 2 32401038; e-mail address: nada.beronska@savba.sk

ramic decreased, when the spark was extinguished or when the arc/spark moved to another surface location. Although the metal melted and vaporized initially, it tended to re-solidify quickly back to surface after spark had disappeared. Norasetthekul et al. found that the Cu/ZrB₂ electrode has the highest thermal wear resistance to the plasma spark at the condition of extremely high energy flux. The electrode could cut the steel workpiece faster than graphite and copper shaping tools [6]. A large difference between the melting point of Cu and ZrB₂ tended to the different erosion mechanism in comparison with the pure elemental electrode. The difference in the type of infiltrated copper was thus not important to the performance of the electrode as long as the melting point of the copper was well below that of the ZrB₂ phase.

The densification of ZrB₂ powder to preform manufacturing is difficult due to its high melting temperature, strong covalent bonds, and low self-diffusivity. Generally, ZrB₂ can be fully densified only at very high sintering temperatures (~2000 °C) and when the external pressure is used. The ZrB₂ powder is coated with zirconium and boron oxides which promotes evaporation and condensation mechanism that results in mass transfer without densification. Several additives have been used to improve densification. Sintering aids (Fe, Ni, Co) are usually used to enhance the sinterability of ZrB₂, but their low melting points restrict high-temperature applicability. Transition metal silicides such as MoSi₂, TaSi₂, WSi₂, TiSi₂, CrSi₂, ZrSi₂, etc. improved densification of ZrB₂ [10–12]. Mishra in [11] investigated the effect of TiC and C additions on sintering behaviour of ZrB₂. He described that small amounts of C and TiC additions (up to 5 %) improve the density of ZrB₂. Another effective way to improve ZrB₂ densification and oxidation resistance was to add the SiC ceramics.

However, the susceptibility to brittle fracture and poor thermal shock resistance of ZrB₂-SiC ceramics limit their potential for using in structural applications [13]. To it, SiC as a typical semiconducting material may limit its electrical applications due to the low electrical conductivity of ceramics [14]. Ahmadi [15] et al. described ZrB₂-SiC composite ceramics which had been doped with different amounts of Si₃N₄ as additive aid. Increasing amounts of Si₃N₄ elevated the formation of gaseous products. Si₃N₄ dopant boosted the sinterability via the formation of interfacial ZrC phase between the particles. Khanra [16] directly tried to develop the ZrB₂-40 wt.% Cu composite by pressureless sintering at 1250 °C for EDM study. The composite shows more metal removal rate with lesser tool removal rate than conventional Cu tool. Finally, whether sintering aids improve sinterability of ZrB₂ or not, the thermal and electrical properties (thermal expansion, thermal conductivity, and electrical conductivity), structural (mechanical) properties, and the sta-

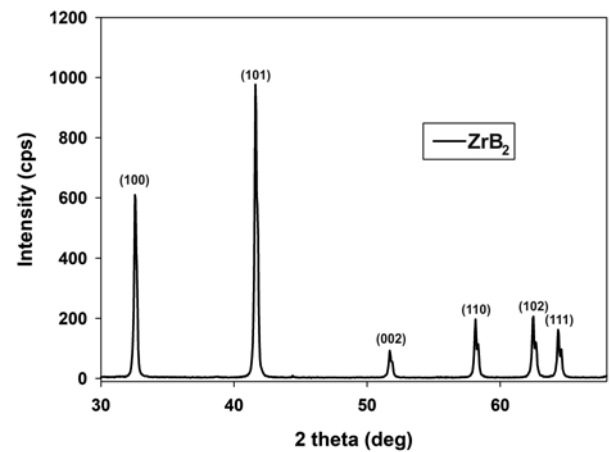


Fig. 1. XRD analysis of the structure of ZrB₂ powder.

bility at high temperatures are mostly negatively influenced. Therefore, much attention has to be focused to prepare composite material in some other way. The infiltration of ZrB₂ powders by molten metal could be more efficient.

This paper presents ZrB₂ powder as a ceramic reinforcement of metal matrix composite infiltrated with molten pure copper and molten copper alloy CuCr1Zr. ZrB₂ powder has the potential to improve the thermal conductivity of Cu/ZrB₂ composite. The question is if the composite is thermally stable. Achieved results of prepared composites are discussed.

2. Materials and methods

Two types of composites Cu/ZrB₂, resp. CuCr1Zr/ZrB₂ were prepared. Commercial ZrB₂ ultrafine powder of particle size lower than 5 μm (*D*₅₀ = 2.8 μm) from Guangzhou Hongwu Material Technology Co., Ltd. was used. The obtained ZrB₂ powder was characterized by X-ray diffraction (Bruker AXS D4 Endeavor diffractometer with Bragg-Brentano geometry and Cu Kα radiation). Both pure Cu and CuCr1Zr alloys were produced by Deutsches Kupferinstitut. The nominal chemical composition of the CuCr1Zr alloy was as follows: Cr (0.5–1.2 %), Zr (0.03–0.3 %), Fe (0.08 %), Si (0.1 %), and Cu (rest). The chemical composition of the copper alloy was confirmed using light emission spectrometry (SPECTROMAX x LMX06) as well as energy dispersive X-ray spectroscopy (EDS-X-Maxx Oxford Instruments).

Both composites were prepared by gas pressure infiltration technology. The ZrB₂ powder infiltrated by pure copper was inserted into the graphite container. The details of the Cu/ZrB₂ infiltration technique have been published in the previous paper [1]. However, the ZrB₂ powder infiltrated by molten copper alloy was fixed in the molybdenum container. Subsequently, the

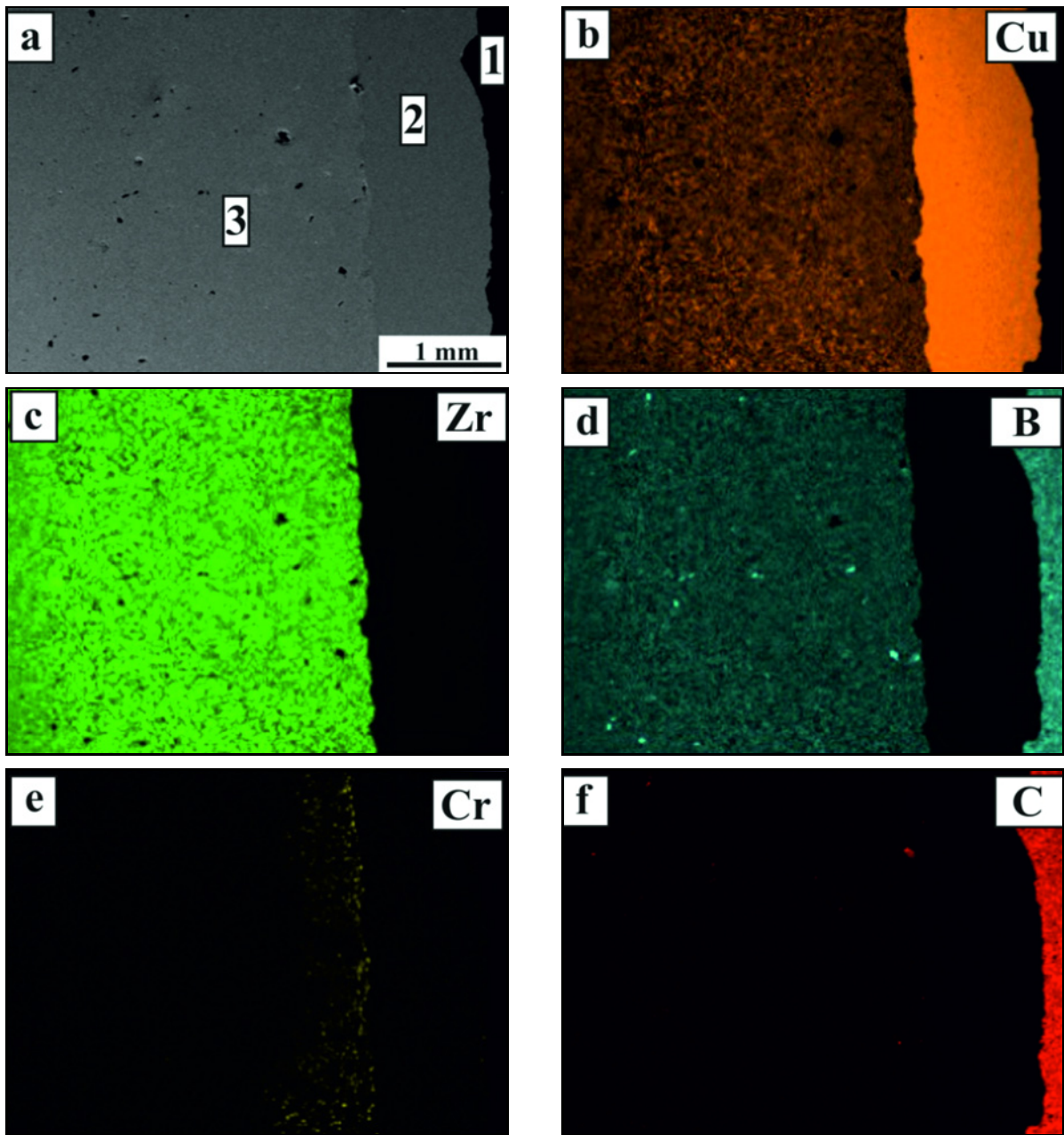


Fig. 2 EDX elemental mapping as-obtained from the contact region between CuCr1Zr/ZrB₂ composite and graphite container (1. graphite container, 2. CuCr1Zr layer, 3. infiltrated powders with CuCr1Zr).

Table 1. The chemical composition of applied Cu and CuCr1Zr alloy as-obtained by light emission spectroscopy (wt.%)

| CuCr1Zr alloy | Cu | Cr | Zr | Fe | Si | Zn | Ni |
|---------------|------|-------|-------|-------|-------|-------|------|
| | 98.9 | 0.756 | 0.134 | 0.049 | 0.022 | 0.015 | 0.01 |

| Cu | Cu | Zn | Fe |
|----|------|-------|-------|
| | 99.9 | 0.014 | 0.015 |

molybdenum container was placed into the bottom part of graphite crucible together with copper alloy. The crucible had been inserted into a high-pressure autoclave and preheated in a vacuum of ~ 60 Pa. The infiltration temperature was 1220 °C. Infiltration of both composites runs under the nitrogen gas due to no wetting [17] and the lack of chemical activity in the Cu/ZrB₂ binary system resulting in poor bonding at the interface. Nitrogen gas pressure was applied up to 5.2 MPa within 300 s. Samples were pulled out from the molten matrix and cooled down in autoclave outside the heated zone.

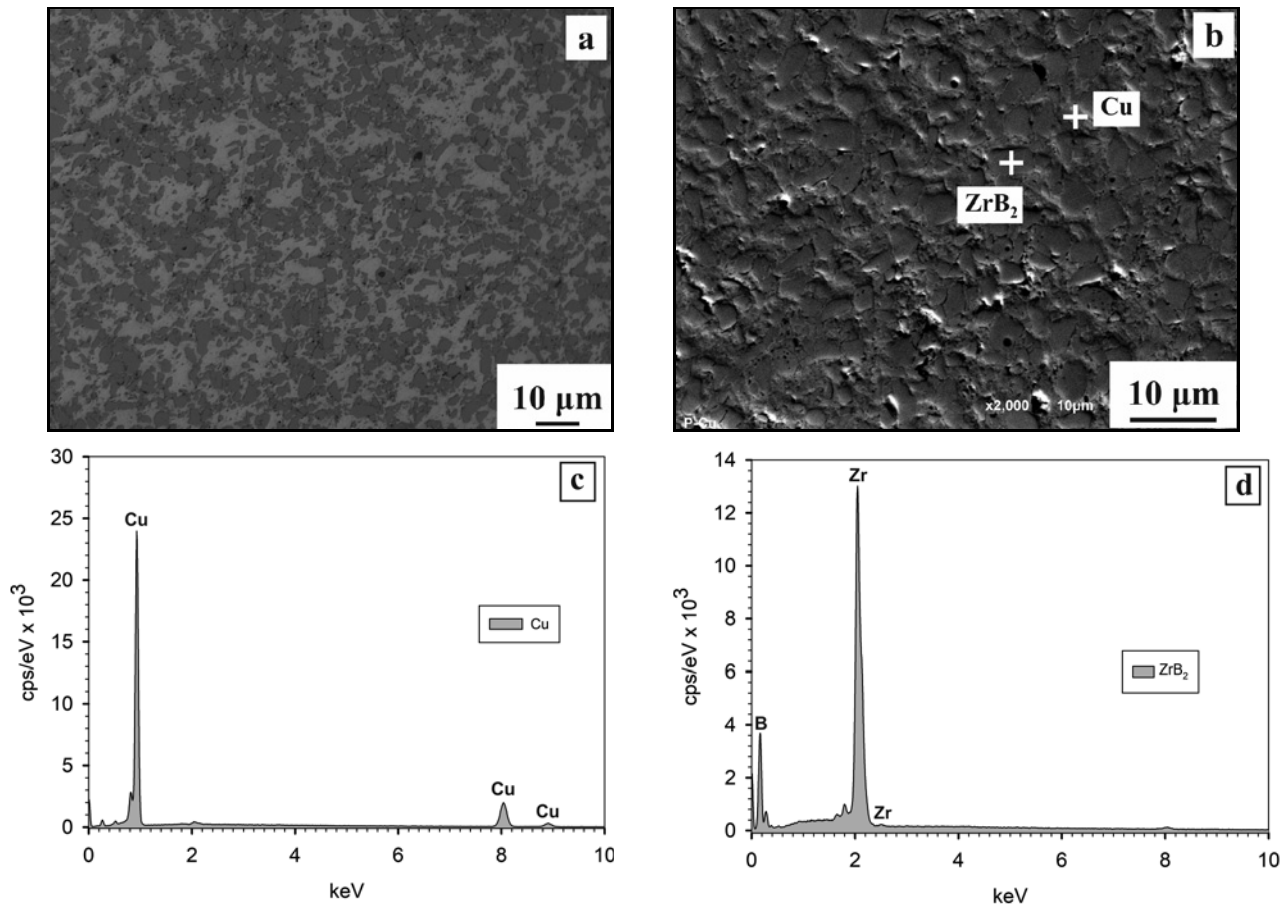


Fig. 3. The microstructure of Cu/ZrB₂ composite as revealed by LM (a), SEM (b), EDX spectra obtained by point analysis in Cu (c), and ZrB₂ (d).

Structural and morphological observations on as-received samples were performed with light microscopy (LM – OLYMPUS GX51) and secondary electron microscopy (SEM – JEOL JSM 6610). Chemical compositions of microstructural phase constituents were determined using energy dispersive X-ray spectroscopy (EDS – X-Maxx Oxford Instruments). Transmission electron microscopy (TEM) observations using a JEOL TEM 1200EX microscope operated at 100 kV were performed to reveal the composite interfaces. Thin foils for TEM studies were prepared using mechanical grinding followed by ion milling with a GATAN PIPS II machine.

The thermal expansion measurements were used to test the thermal stability of composites. Samples with the dimensions of $4 \times 4 \times 10 \text{ mm}^3$ were subjected to 5 consecutive heating and cooling cycles at the heating/cooling rate of 3°C min^{-1} in an argon atmosphere using NETZSCH DIL 402 Expedia Select dilatometer equipped with an alumina holder. Samples were cycled in the temperature range from 30 to 800°C . Instantaneous CTE values were calculated from the strain-temperature curves.

3. Results and discussion

3.1. Powder and alloy characterization

The X-ray diffraction analysis of ZrB₂ ultrafine zirconium diboride powder revealed the purity and the crystal structure of the ZrB₂ powder used in experiments. The measurement of the ZrB₂ powders confirmed pure hexagonal crystal structure according to PDF 00-034-0423 [18] as is presented in Fig. 1.

The chemical composition of applied Cu and CuCr1Zr alloy as obtained by light emission spectroscopy is presented in Table 1. The measurements confirmed the limits declared by the supplier.

3.2. Gas pressure infiltration method

Cu/ZrB₂ was infiltrated without any difficulties. CuCr1Zr was used in order to improve the interface between composite constituents. Our first tests with copper alloy indicated that the infiltration of CuCr1Zr into the ZrB₂ powder was not possible when graphite container was used. After infiltration of ZrB₂ powder with copper alloy placed in a graphite container, no Cr

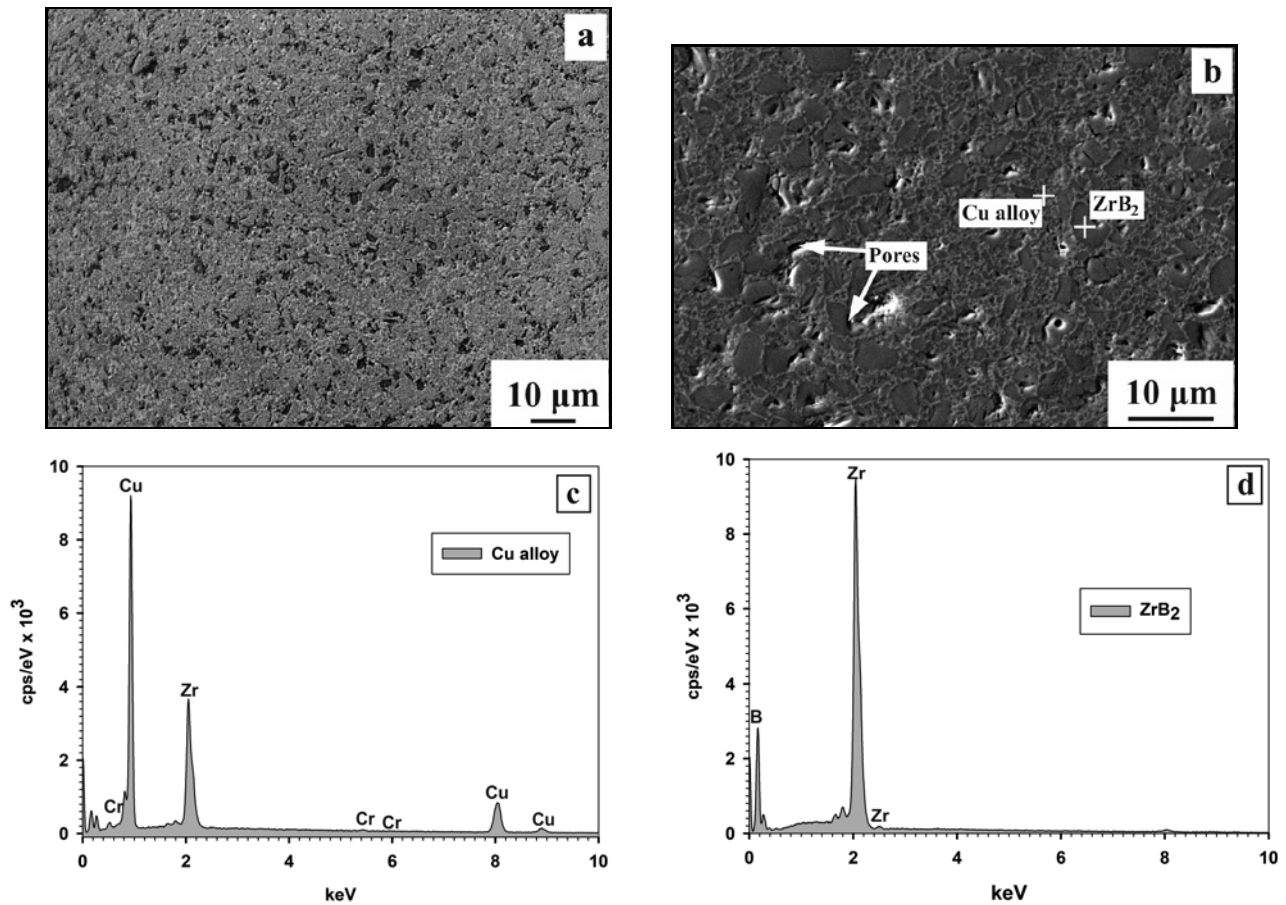


Fig. 4. The microstructure of CuCr1Zr/ZrB₂ composite as revealed by LM (a), SEM (b), EDX spectra obtained by point analysis in CuCr1Zr (c), and ZrB₂ (d).

in the whole volume of CuCr1Zr/ZrB₂ composite sample was detected using SEM-EDS analysis. As can be seen from the EDS map in Fig. 2, the presence of large quantities of Cr was observed in the places with the contacts of the sample with a graphite wall of the container. It can be supposed that Cr primarily reacted with carbon from the graphite container to form the reaction product of chromium carbide [19]. As the solution to avoid the Cr reaction with graphite, the powders were placed into Mo container. Subsequently, Mo container was placed in a graphite crucible and then infiltrated.

3.3. Structural studies

Microstructural studies were performed by LM, SEM, and TEM (Figs. 3–5). The microstructure of Cu/ZrB₂ composite as revealed by LM is presented in Fig. 3a. The copper appears light and ZrB₂ ceramics dark. The similar microstructure was observed at the top and bottom of the infiltrated samples. This proved that copper did sufficiently penetrate the whole volume of the sample. Therefore, it is evident that Cu/ZrB₂ composites were homogeneous throughout

the whole sample. Although some pores were rarely observed, neither zones without Cu, nor cracks, cavities and other defects with negative effect on the microstructure and thus the thermal properties were observed. The composite structure as revealed by SEM presented in Fig. 3b is confirming the results obtained by LM observations. The EDX spectra corresponding to Cu and ZrB₂ are presented in Fig. 3c, resp. 3d.

The microstructure of CuCr1Zr/ZrB₂ composite as revealed by LM is presented in Fig. 4a. The copper appears light and ZrB₂ ceramics dark. The microstructure at the top of the sample compared to the bottom was similar. Copper did penetrate the whole volume of the composite sample, and the CuCr1Zr/ZrB₂ composite revealed the homogeneous structure throughout the whole sample. Only about ~1.6% of pores were observed. However, no zones without Cu, or structural inhomogeneities, e.g. cracks, cavities, and other defects with negative effect on the microstructure and thus the thermal properties were observed. The composite structure as revealed by SEM presented in Fig. 4b is confirming the results obtained by LM observations. The EDX spectra corresponding to CuCr1Zr and ZrB₂ are presented in Figs. 4c and 4d.

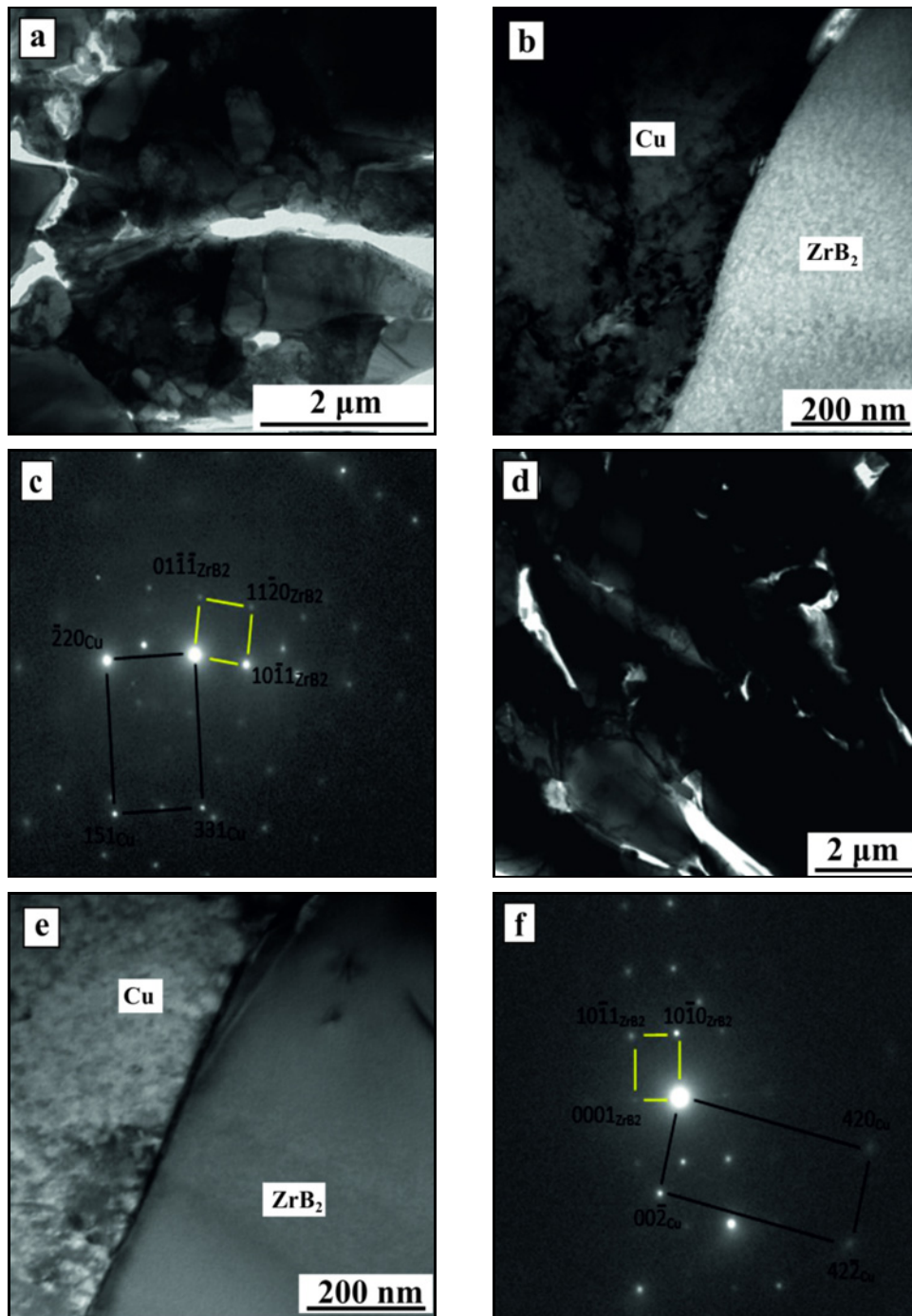


Fig. 5. TEM micrographs: (a) Cu/ZrB₂ microstructure; (b) Cu/ZrB₂ interface; (c) SAED of interface area; (d) CuCr1Zr/ZrB₂ microstructure; (e) CuCr1Zr/ZrB₂ interface; (f) SAED of interface area.

The detection of the chemical composition of the Cu-ZrB₂ and CuCr1Zr-ZrB₂ composites after infiltration was determined by EDX from 3 area measurements, shown in Table 2, resp. Table 3.

Generally, no reaction zones or phases were revealed by TEM studies of composites' interfacial zones. The microstructures in Fig. 5a, resp. 5d show distributed ZrB₂ powders surrounded with the matrix Cu, resp. CuCr1Zr. The higher amount of micro-

pores in the microstructure is also evident. Discreet interfaces of ZrB₂ powder and matrix metals as revealed in Fig. 5b, resp. 5e are observed. The selected area electron diffraction (SAED) pattern taken from the ZrB₂-matrix interfacial region contains diffraction spots from both the ZrB₂ and copper matrix (Fig. 5c, resp. 5f). The orientation relationship is $\langle -1-16 \rangle_{\text{Cu}} // \langle 1-11 \rangle_{\text{ZrB}_2}$. The composite with CuZr1Cr alloy also shows distinguished borders with

Table 2. Results of statistics of EDX chemical composition of Cu-ZrB₂ composite (wt.%)

| | B | Cu | Zr |
|--------------------|-------|-------|-------|
| Max | 31.50 | 36.43 | 37.51 |
| Min | 27.93 | 32.03 | 35.64 |
| Average | 30.15 | 33.34 | 36.52 |
| Standard deviation | 1.59 | 2.7 | 0.77 |

Table 3. Results of statistics of EDX chemical composition of CuCr1Zr-ZrB₂ composite (wt.%)

| | B | Cr | Cu | Zr |
|--------------------|-------|------|-------|-------|
| Max | 30.85 | 0.94 | 38.42 | 31.45 |
| Min | 29.64 | 0.64 | 37.12 | 31.00 |
| Average | 30.30 | 0.81 | 37.68 | 31.21 |
| Standard deviation | 0.61 | 0.16 | 0.67 | 0.23 |

no interfacial reaction with orientation relationship $\langle 1-20 \rangle_{\text{Cu}} // \langle 010 \rangle_{\text{ZrB}_2}$.

3.4. Thermal expansion

Thermal expansion measurements are sensitive to any phase changes in the tested material, and repeated heating/cooling cycles indicate the structural stability of the composite subjected to thermal stresses resulting from different coefficients of thermal expansion.

The temperature dependences of relative elongation with corresponding coefficients of thermal expansion for Cu/ZrB₂ composite, pure Cu and ZrB₂ as references are presented in Fig. 6. As a ZrB₂ reference, the thermal behaviour of ZrB₂ preform measured in the previous paper was taken into account [1]. The thermal expansion in the first cycle is slightly different when compared to 2–5. This is due to the release of manufacturing thermal stresses built during the cooling from the infiltration temperature 1220 °C. The CTE of the Cu/ZrB₂ powder composite is higher when compared with pure ZrB₂, but substantially lower than that of reference Cu. Demonstrating this ZrB₂ contribution in the composite moves the CTE to lower values. However, CTE linear decreases in the temperature range 510 to 630 °C were observed in both composites and ZrB₂ reference (Fig. 6b, resp. 7b). It is apparent that the deflection in CTE curve is similar indicating that the ZrB₂ qualitatively rules the thermal expansion.

Chemical analysis confirmed the composition of Cu, CuCr1Zr, and ZrB₂ constituents. The binary B-Zr diagram in [20] shows that ZrB₂ compound ex-

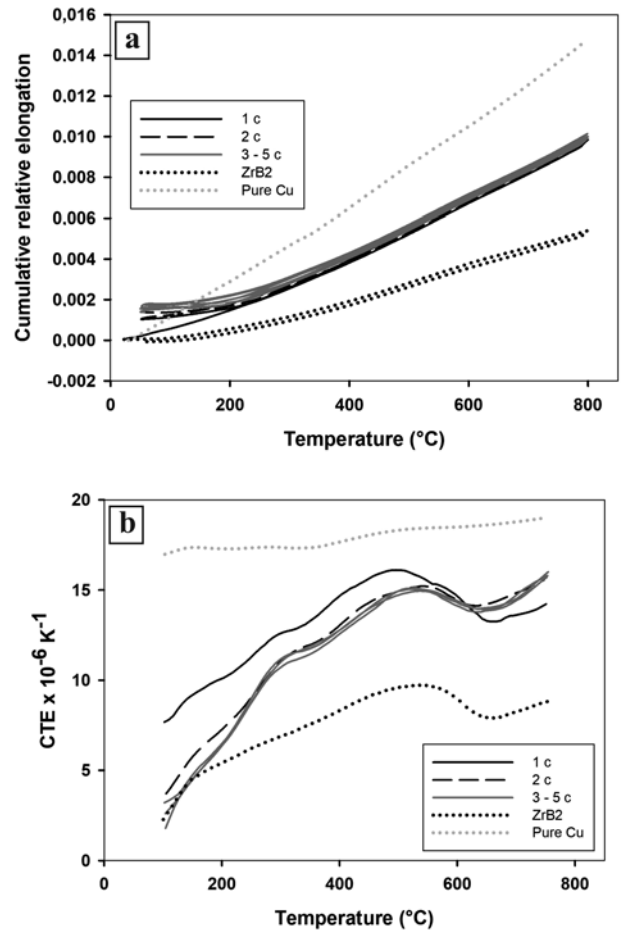


Fig. 6. Cumulative relative elongations (a) and coefficients of thermal expansion (b) of the Cu/ZrB₂ composite in comparison with pure Cu and ZrB₂ references.

ists in a very narrow concentration range and there are no phase changes up to its melting point. The reason for the observed deviation in CTE in the temperature range 510 to 630 °C that was recorded for ZrB₂ bulk as well as for both composites resulted from the anisotropic hexagonal structure of ZrB₂. The crystal arrangement of ZrB₂ is hexagonal with alternating layers of Zr and B atoms. This hexagonal nature of ZrB₂ leads to its anisotropic behaviour and properties. Paxton et al. [21] observed anisotropic behaviour with a larger CTE in the *c*-axis. Two lines converge to the same value at around 780 K (507 °C), where the CTE is isotropic. At the temperatures higher than 507 °C they observed a higher expansion in the *a*-axis. As the observed deviation in CTE is in the vicinity of these temperatures, it is quite probable that it is to be related to this anisotropy in the thermal expansion of ZrB₂ itself.

The temperature dependences of relative elongation with corresponding coefficients of thermal expansion for Cu/Cr1Zr/ZrB₂ composite, Cu alloy, and

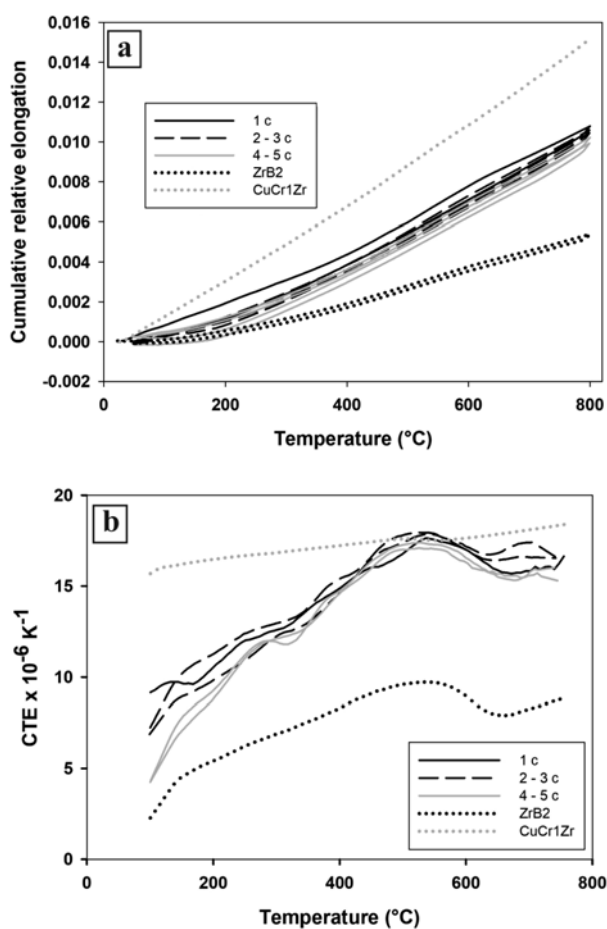


Fig. 7. Cumulative relative elongations (a) and coefficients of thermal expansion (b) of the CuCr1Zr/ZrB₂ composite in comparison with CuCr1Zr and ZrB₂ references.

ZrB₂ as references are presented in Fig. 7. Both dependences are qualitatively quite similar to the Cu/ZrB₂ curves demonstrated in Fig. 6. It indicates that the

thermal expansion behaviour of pure Cu, as well as CuCr1Zr matrix, is comparable. It can be supposed that the porosity does not have much of an effect on the CTEs of composites. This is in agreement with results [22] where Choe et al. confirmed that the CTE was independent of porosity for anisotropic materials.

No interfacial reaction took place for Cu neither for CuCr1Zr matrix. The interfacial bonding can be therefore regarded as non-reactive nature. Despite these facts, the thermal stability of the composites is quite good without any indication of possible disintegration. It is clear that the lowest CTE exhibits the ZrB₂ reference followed by both composites and both metal matrix (Fig. 6b, resp. 7b). All measurements of thermal expansions confirmed the results with infiltrated ZrB₂ preforms [1].

Maximums of elongations recorded for particular heating/cooling cycles slightly increased for Cu/ZrB₂ composite and slightly decreased for CuCr1Zr/ZrB₂ composite (Fig. 8). This indicates that the stability of the composite with CuCr1Zr matrix somewhat improves when subjected to the applied thermal cycling. Apart from this result, the differences between Cu/ZrB₂ and CuCr1Zr/ZrB₂ composites are negligible.

4. Conclusions

Cu/ZrB₂ and CuCr1Zr/ZrB₂ composites were successfully prepared by gas pressure infiltration of ZrB₂ powders. No substantial differences in the behaviour of composites were observed due to the matrix compositions. No interfacial reaction was observed indicating that the bonding was non-reactive. Both composites exhibited high structural stability when subjected to 5 consecutive heating/cooling cycles to 800°C. It can be supposed that the porosity does not have much of an effect on the CTEs of composites.

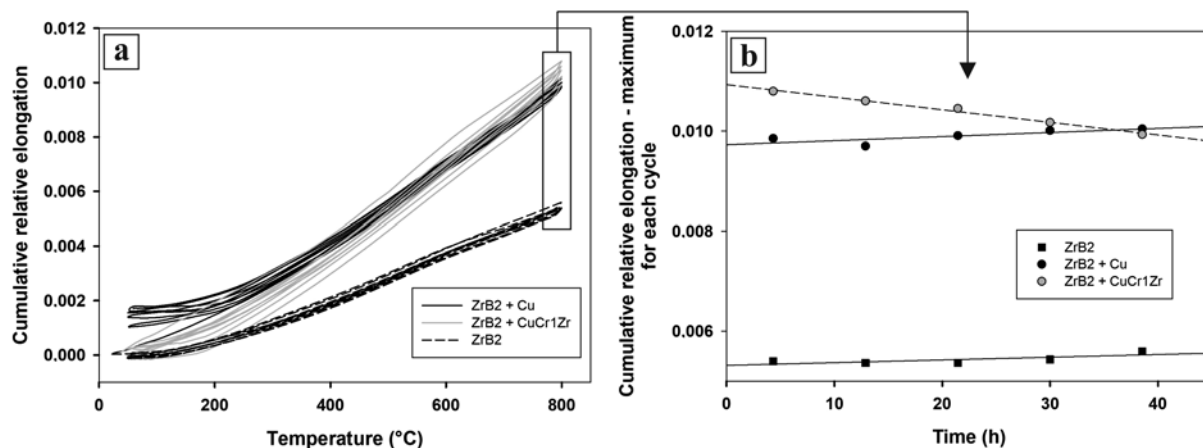


Fig. 8. Temperature dependences of thermal expansion (a) and maximum elongations recorded for particular cycles (b).

Acknowledgement

This work was supported by the Slovak Scientific Grant Agency (grant number VEGA 2/0172/16).

References

- [1] Opálek, A., Beronská, N., Nagy, Š., Dvorák, T., Štefánik, P., Švantner, T., Švec, P., Iždinský, K.: *Kovove Mater.*, 57, 2019, p. 1. [doi:10.4149/km_2019_1_1](https://doi.org/10.4149/km_2019_1_1)
- [2] Nasiri, Z., Mashhadi, M.: *Int. J. Refract. Metals Hard. Mater.*, 78, 2019, p. 186. [doi:10.1016/j.ijrmhm.2018.09.009](https://doi.org/10.1016/j.ijrmhm.2018.09.009)
- [3] Zimmermann, J. W., Hilmas, G. E., Fahrenholtz, W. G., Dinwiddie, R. B., Porter, W. D., Wang, H.: *J. Am. Ceram. Soc.*, 91, 2008, p. 1405. [doi:10.1111/j.1551-2916.2008.02268.x](https://doi.org/10.1111/j.1551-2916.2008.02268.x)
- [4] Monteverde, F., Bellosi, A., Guicciardi, S.: *J. Eur. Ceram. Soc.*, 22, 2002, p. 279. [doi:10.1016/S0955-2219\(01\)00284-9](https://doi.org/10.1016/S0955-2219(01)00284-9)
- [5] Das, J., Suraj, P., Kumar, D. S. S., Shekhar, L., Pruthvi, J., Kumari, S., Srinivas, V., Reddy, J. J., Prasad, V. V. B.: *Int. J. Refract. Metals Hard. Mater.*, 69, 2017, p. 49. [doi:10.1016/j.ijrmhm.2017.08.001](https://doi.org/10.1016/j.ijrmhm.2017.08.001)
- [6] Norasethekul, S., Eubank, P. T., Bradley, W. L., Bozkurt, B., Stucker, B.: *J. Mater. Sci.*, 34, 1999, p. 1261. [doi:10.1023/A:1004529527162](https://doi.org/10.1023/A:1004529527162)
- [7] Khanra, A. K., Sarkar, B. R., Bhattacharya, B., Pathak, L. C., Godkhindi, M. M.: *J. Mater. Process. Tech.*, 183, 2007, p. 122. [doi:10.1016/j.jmatprotec.2006.09.034](https://doi.org/10.1016/j.jmatprotec.2006.09.034)
- [8] Guo, D., Zhang, M., Jin, Z., Kang, R.: *J. Mater. Sci. Technol.*, 22, 2006, p. 514.
- [9] Stucker, B., Bradley, W., Eubank, P. T., Norasethekul, S., Bozkurt, B.: In: *Proceedings of the International Solid Freeform Fabrication Symposium*. Austin, the University of Texas at Austin 1997, p. 257.
- [10] Zhang, S., Wang, S., Li, W., Zhu, Y., Chen, Z.: *Mater. Lett.*, 65, 2011, p. 2910. [doi:10.1016/j.matlet.2011.06.070](https://doi.org/10.1016/j.matlet.2011.06.070)
- [11] Mishra, S. K., Das, S. K.: *Mater. Lett.*, 59, 2005, p. 3467. [doi:10.1016/j.matlet.2005.06.015](https://doi.org/10.1016/j.matlet.2005.06.015)
- [12] Sonber, J. K., Murthy, T. S. R. Ch., Sairam, K., Nagaraj, A., Majumdar, S., Kain, V.: *Int. J. Refract. Metals Hard. Mater.*, 70, 2018, p. 56. [doi:10.1016/j.ijrmhm.2017.09.013](https://doi.org/10.1016/j.ijrmhm.2017.09.013)
- [13] Hu, P., Gui, K., Hong, W., Zhang, X., Dong, S.: *J. Eur. Ceram. Soc.*, 37, 2017, p. 2317. [doi:10.1016/j.jeurceramsoc.2017.02.008](https://doi.org/10.1016/j.jeurceramsoc.2017.02.008)
- [14] Chen, J., Chen, J., Chen, Z., Liu, X., Huang, Z., Huang, Y.: *J. Eur. Ceram. Soc.*, 38, 2018, p. 2477. [doi:10.1016/j.jeurceramsoc.2018.01.020](https://doi.org/10.1016/j.jeurceramsoc.2018.01.020)
- [15] Ahmandi, Z., Nayebi, B., Asl, M. S., Kakroudi, M. G., Farahbakhsh, I.: *Ceram. Int.*, 43, 2017, p. 9699. [doi:10.1016/j.ceramint.2017.04.144](https://doi.org/10.1016/j.ceramint.2017.04.144)
- [16] Khanra, A. K., Pathak, L. C., Godkhindiet, M. M.: *B. Mater. Sci.*, 32, 2009, p. 401. [doi:10.1007/s12034-009-0058-0](https://doi.org/10.1007/s12034-009-0058-0)
- [17] Muolo, M. L., Ferrera, E., Novakovic, R., Passerone, A.: *Scripta Mater.*, 48, 2003, p. 191. [doi:10.1016/S1359-6462\(02\)00361-5](https://doi.org/10.1016/S1359-6462(02)00361-5)
- [18] International Centre for Diffraction Data. PDF Number: 00-034-0423. <http://www.icdd.com/index.php/pdfsearch/>
- [19] Beronská, N., Iždinský, K., Štefánik, P., Šimančík, F., Zemánková, M., Dvorák, T.: *Kovove Mater.*, 47, 2009, p. 175.
- [20] Franke, P., Neuschütz, D. (Eds.): *Binary Systems. Part 5: Binary Systems Supplement 1. Landolt-Börnstein – Group IV Physical Chemistry (Numerical Data and Functional Relationships in Science and Technology)*. Berlin, Heidelberg, Springer 1995.
- [21] Paxton, W. A., Özdemir, T. E., Şavklyıldız, İ., Whalen, T., Biçer, H., Akdoğan, E. K., Zhong, Zh., Tsakalakos, Th.: *J. Ceram.*, 2016, 2016, ID 8346563. [doi:10.1155/2016/8346563](https://doi.org/10.1155/2016/8346563)
- [22] Choe, H., Hsieh, T., Wolfenstine, J.: *Mater. Science and Eng. A*, 327, 1997, p. 250.